MDPI

Article

Uncertainty-Estimation-Based Prescribed Performance Pressure Control for Train Electropneumatic Brake Systems

Rui Zhang [1,†]**, Zejun Xu** [1,†]**, Yingze Yang** [2,†] **and Peidong Zhu** [1,*]

1. School of Electronic Information and Electrical Engineering, Changsha University, Changsha 410022, China; ruizhang@ccsu.edu.cn (R.Z.); zejunxu@163.com (Z.X.)
2. School of Computer Science and Engineering, Central South University, Changsha 410083, China; yangyingze@csu.edu.cn
* Correspondence: zpeidong@126.com
† These authors contributed equally to this work.

Abstract: Fast and precise pressure control for an electropneumatic brake system is essential for ensuring the safe operation of trains. However, the nonlinearity and uncertainties of the system make controller design challenging. This paper proposes a prescribed performance control method integrating an extended state observer to address this issue. A thermodynamical model of the brake cylinder is first built based on the pneumatic characteristics of the braking system, considering multiple modes, coupling effects, and input saturation. Then, an extended state observer is designed to estimate model uncertainty due to temperature variation and disturbances and to achieve online compensation of the model. A feedback control law with a specified prescribed performance function is developed based on the updated thermodynamic model to guarantee the transient and steady-state performance of the pressure control. A parameter adaptive method is also utilized to handle input saturation. The observer's bounded convergence and stability analysis of the closed-loop control system is given using the Lyapunov theory. Compared experimental results are provided to verify the effectiveness of the proposed method.

Keywords: electropneumatic brake system; prescribed performance; uncertainty estimation; extended state observer; input saturation

1. Introduction

The electropneumatic brake system is crucial for ensuring the safe operation of trains. One critical issue is implementing the fast and precise pressure tracking control of the brake cylinder in the electropneumatic brake system [1]. However, some intrinsic characteristics significantly challenge the reliable and robust pressure control of the electropneumatic brake system. First, the system presents time-varying dynamics because the temperature within the airtight brake cylinder is inherently varying due to the thermal effect during the pressure regulation process. Specifically, due to the compressibility of air during the charging and discharging process, the changed pressure causes the air temperature in the brake cylinder to vary rapidly in a short time [2]. In reverse, the varying temperature resulting from the pressure change significantly affects the pressure response of the brake cylinder. The coupling between the pressure and the air temperature complicates the system dynamics. Moreover, in the electropneumatic brake system, the discrete nature of on/off solenoid valves and the high nonlinearity caused by the air compressibility, airflow, and disturbances also increase the difficulty of accurate pressure control [3].

There has been much research on the pressure-tracking control of electropneumatic systems. As the classical linear control method, proportional–integral–differential control has been widely used in pneumatic systems due to its simple structure and convenient deployment [4]. However, for a pneumatic system with strong nonlinearity, the transient and steady-state performances of pneumatic systems cannot always be guaranteed with

proportional–integral–differential control. Some model-based nonlinear control methods such as sliding mode control [5,6] and model predictive control [7,8] were also proposed to regulate the pressure of electropneumatic actuators. For these methods, the control performance is strongly dependent on the accuracy of the model. Nevertheless, the accurate pressure dynamic model of the brake system is challenging to construct, and the model parameters are uncertain due to the complex thermal effects [9].

It is common to introduce observer-based estimation methods to address these uncertainties. A sliding-mode observer was developed in [10] to estimate the unknown time-variant temperature of pneumatic systems. However, it has a chattering effect and cannot provide enough estimation accuracy when the temperature changes rapidly. A dynamic nonlinear high-gain observer was developed in [11] to estimate the air temperature of a small pneumatic actuator, while the effect of disturbance is hard to overcome. Thus, it is necessary to develop an appropriate method to estimate the uncertain temperature and disturbances for the train electropneumatic brake system.

The extended state observer developed by Jingqing Han can deal with external disturbances and uncertain system dynamics simultaneously [12]. It takes the system uncertainty and disturbances as a new state variable to estimate, and it achieves this without requiring exact model information [13]. For this purpose, the extended state observer has been applied in many practical engineering applications. For instance, in [14], an extended state observer was proposed to estimate slip ratio, train adhesion, and system uncertainties for active braking control of high-speed trains. In [15], an adaptive fast-finite-time extended state observer was designed to estimate the unmeasured state variables, external disturbances, and uncertainties of electro-hydraulic actuator systems. Motivated by the advantages of the extended state observer, the uncertain temperature variation and the disturbances can be estimated simultaneously by the extended state observer and then compensated in the pressure control of the train electropneumatic system.

During the train braking process, it is critical to ensure the pressure control performance, such as improving the tracking speed, reducing the overshoot, and decreasing the steady-state error, so that the rapidity, smoothness, and accuracy of train braking can be guaranteed. In some existing pneumatic pressure control methods for trains, such as sliding mode control [5] and model predictive control [8], it is difficult to achieve the performance constraint quantitatively. The prescribed performance control developed by Bechlioulis et al. [16] is a promising method for a performance guarantee. The core idea of the control method is to apply a specified prescribed performance function on the tracking error system. The prescribed performance function characterizing the convergence rate, maximum overshoot, and steady-state error is used for the tracking error transformation. If the transformed error system is controlled to be stable, the tracking error of the original system will be guaranteed within the prescribed bound. The prescribed performance control method has been successfully applied to various industrial applications, such as the trajectory tracking problem of a three-degree-of-freedom helicopter [17], the trajectory tracking control of an unmanned surface vehicle [18], and so on.

In this paper, a prescribed performance control method based on the extended state observer is proposed for the fast and precise pressure tracking control of the brake cylinder in a train electropneumatic brake system. First, considering the uncertainties caused by the thermal effect and disturbances, high nonlinearity, and input saturation, a novel thermodynamic model of the brake cylinder is proposed to describe the pressure dynamics. Then, an extended state observer is designed to estimate the uncertainties caused by the in-cylinder temperature variation and disturbances. Afterwards, a feedback control law is designed to make the pressure control system achieve the desired performance requirements by introducing a prescribed performance function. Moreover, a parameter adaptive method is developed to address the input saturation issue. The stability of the proposed observer and controller is analyzed rigorously in the paper. The compared experimental results are provided to verify the validity of the proposed pressure control method.

The main contributions of this paper are summarized as follows:

- A comprehensive pressure dynamical model is developed for the train electropneumatic system, taking into account its multiple operating modes, uncertainties, and control input saturation for the first time.
- The design of an extended state observer is carried out to estimate the unknown dynamics of the brake cylinder, which includes uncertain temperature and disturbances. The estimated uncertainty is then used to update the system's thermodynamic model to ensure the accuracy of the system model, thereby facilitating the controller design. Additionally, a thorough analysis of the estimator's convergence is conducted.
- A novel pressure feedback controller for the train electropneumatic system is proposed by combining a specified prescribed performance function and a parameter adaptive method. This controller can handle the system's nonlinearity, uncertainty, and input saturation, improving transient and steady-state performances. The stability of the closed-loop system is proven using the Lyapunov theory.

The rest of this paper is organized as follows. In Section 2, the characteristics of the train electropneumatic brake system are analyzed, and the system model is constructed consequently. Section 3 presents the online model uncertainty estimation based on an extended state observer. Using the estimated uncertainty and the prescribed performance control method, we design a pressure feedback controller in Section 4. The experimental results are provided in Section 5. The paper is concluded in Section 6.

2. System Description and Modeling

2.1. Description of Train Electropneumatic Brake System

The train electropneumatic brake system under study is shown in Figure 1. According to the illustration of this figure, once the train driver applies the braking or releasing command, a reference pressure is given first. Then, the pressure controller generates control signals to regulate the states of the supply valve and the exhaust valve so that the air flows in or out of the brake cylinder, making the brake cylinder pressure track the reference values. With the brake cylinder pressure, the corresponding braking force is generated to stop a running train. Thus, the fast and precise pressure tracking control of the brake cylinder is critical for guaranteeing the braking operation of trains.
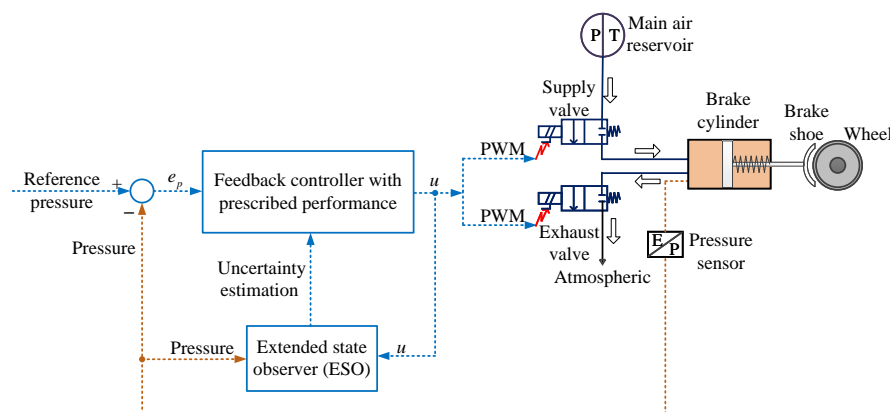
Figure 1. ESO-based prescribed performance pressure control scheme for the train electropneumatic brake system.

2.2. System Model

In the pressure control process of the brake cylinder, there are three valid operating modes according to the states of the supply valve and the exhaust valve. Here, we define three modes as *holding mode*, *charging mode*, and *discharging mode*. In this section, the open-loop dynamic models of the brake cylinder in each mode are described first. Then, a unified averaged continuous input model with input saturation is built to facilitate the controller design.

2.2.1. Pressure Dynamics in the Holding Mode

In the *holding mode*, the supply and exhaust valves are closed. The mass flow rate is zero. Then, the pressure dynamics in this mode are given by

$$\dot{p} = -k_t p + \phi(t), \tag{1}$$

where p is the brake cylinder pressure; $k_t p$ means the pressure variation due to the air leakage and k_t is the coefficient of the total leakage; $\phi(t)$ is the model uncertainties caused by the temperature variation and uncertain disturbances, and so on.

2.2.2. Pressure Dynamics in the Charging Mode

In the *charging mode*, the supply valve is open, and the exhaust valve is closed. The compressed air flows from the main air reservoir to the brake cylinder, and the pressure in the brake cylinder increases. Using the first principle of thermodynamics, the pressure dynamic model of the brake cylinder in the *charging mode* can be described as,

$$\dot{p} = \gamma \frac{RT}{V} q_{m1} - k_t p + \phi(t), \tag{2}$$

where the term $\gamma \frac{RT}{V} q_{m1}$ is the brake cylinder pressure variation caused by the mass flow rate, and the meanings of notations in this term are defined as follows. γ is the ratio of specific heats; R is the gas constant; T is the air temperature of the brake cylinder; V is the total volume of the brake cylinder; q_{m1} is the mass flow rate to the brake cylinder, and it is a nonlinear function of the ratio of the brake cylinder pressure and the main air reservoir pressure given by [19], and it is also subjected to a phenomenon called choking. A critical pressure ratio is typically employed in pneumatic systems to distinguish between choked and unchoked flow.

$$q_{m1} = \frac{p_s C_d A_1}{\sqrt{RT}} \times \begin{cases} \sqrt{\gamma \left(\frac{2}{\gamma+1}\right)^{\frac{\gamma+1}{\gamma-1}}}, \text{if } \frac{p}{p_s} \leq p_c \, (\text{choked flow}) \\ \sqrt{\frac{2\gamma}{\gamma-1}} \sqrt{\left(\frac{p}{p_s}\right)^{\frac{2}{\gamma}} - \left(\frac{p}{p_s}\right)^{\frac{\gamma+1}{\gamma}}}, \text{if } \frac{p}{p_s} > p_c \, (\text{unchoked flow}) \end{cases} \tag{3}$$

where p_s is the main air reservoir pressure, C_d is the flow coefficient, A_1 is the orifice 1 passage area, and p_c is the critical pressure ratio, where its value is generally set as 0.528 [19].

2.2.3. Pressure Dynamics in the Discharging Mode

In the *discharging mode*, the supply valve is closed, and the exhaust valve is open. The compressed air flows from the brake cylinder to the atmosphere, and the pressure in the brake cylinder decreases. The pressure dynamics in this mode are modeled as

$$\dot{p} = -\gamma \frac{RT}{V} q_{m2} - k_t p + \phi(t), \tag{4}$$

where the term $-\gamma \frac{RT}{V} q_{m2}$ is the brake cylinder pressure variation caused by the mass flow rate, and the meanings of notations in this term are defined as follows. q_{m2} is the mass flow rate from the brake cylinder to the atmosphere, and it is a nonlinear function of the ratio of the atmospheric pressure and the brake cylinder pressure given by [19],

$$q_{m2} = \frac{p C_d A_2}{\sqrt{RT}} \times \begin{cases} \sqrt{\gamma \left(\frac{2}{\gamma+1}\right)^{\frac{\gamma+1}{\gamma-1}}}, \text{if } \frac{p_a}{p} \leq p_c \, (\text{choked flow}) \\ \sqrt{\frac{2\gamma}{\gamma-1}} \sqrt{\left(\frac{p_a}{p}\right)^{\frac{2}{\gamma}} - \left(\frac{p_a}{p}\right)^{\frac{\gamma+1}{\gamma}}}, \text{if } \frac{p_a}{p} > p_c \, (\text{unchoked flow}) \end{cases} \tag{5}$$

where p_a is the atmospheric pressure and A_2 is the orifice 2 passage area. The meanings of other notations in (4) and (5) are the same as those in (2) and (3).

It is worth noting that the brake cylinder is a diaphragm-operated actuator, and it is approximated by a single-acting pneumatic cylinder, as shown in Figure 1. From this figure, the volume V changes in the charging and discharging modes. Therefore, the $\phi(t)$ in Formulas (2) and (4) also include the uncertainty caused by the changed brake cylinder volume.

2.2.4. Unified Model

In a real train electropneumatic brake system, on/off solenoid valves are driven by controlling the input voltages. Thus, we propose to design a continuous-time controller for controlling solenoid valves and achieving pressure tracking. For this purpose, a unified averaged continuous-input model should be built. The practical system input for the electropneumatic brake system is the pulse width modulation, which is constrained within the region $[-1, 1]$. Using the nonlinear model averaging approach given in [20], an averaged model for describing the pressure dynamics of the brake cylinder is constructed as

$$\dot{p} = b(u_c, p)u_c + g(p) + \phi(t), \tag{6}$$

where $g(p) = -k_t p$, u_c is the practical control input,

$$b(u_c, p) = \gamma \frac{RT}{V} \left[q_{m1} \left(\frac{1 + \text{sgn}(u_c)}{2} \right) + q_{m2} \left(\frac{1 - \text{sgn}(u_c)}{2} \right) \right], \tag{7}$$

and $\text{sgn}(\cdot)$ is the sign function.

Further, the practical control input u_c is described by the following saturation function:

$$u_c = sat(u) = \begin{cases} u_m \cdot \text{sgn}(u), & |u| \geq u_m, \\ u, & |u| < u_m, \end{cases} \tag{8}$$

where u denotes the desired control input that will be designed, u_m denotes the input saturation limit, and $sat(\cdot)$ denotes the saturation function.

For Formula (8), there exists a difference Δu between the designed input u and the practical control input u_c. The relationship can be defined as

$$\Delta u = u_c - u = sat(u) - u. \tag{9}$$

From the perspective of a practical control system, system controllability should be satisfied when control input saturation appears [21]. Therefore, we assume that the difference Δu can be regarded as a bounded function, satisfying

$$\|\Delta u\| \leq \Pi(p) \cdot \zeta, \tag{10}$$

where $\Pi(p)$ is a known auxiliary continuous function and ζ is an unknown parameter.

Remark 1. *According to Formula (7), $b(u_c, p)$ is not differentiable at $u_c = 0$ since it contains $\text{sgn}(u_c)$. But, except at the singular point of $u_c = 0$, it is worth noting that $b(u_c, p)$ is always differentiable even it is at $q_{m1} = \dfrac{p_s C_d A_1}{\sqrt{RT}} \sqrt{\gamma \left(\dfrac{2}{\gamma + 1} \right)^{\frac{\gamma+1}{\gamma-1}}}$ with $p = 0.528 p_s$,*

$q_{m2} = \dfrac{p C_d A_2}{\sqrt{RT}} \sqrt{\gamma \left(\dfrac{2}{\gamma + 1} \right)^{\frac{\gamma+1}{\gamma-1}}}$ with $p = p_a/0.528$ and is continuous everywhere because the left and right derivatives of $b(u_c, p)$ at $u_c = 0$ exist and are finite. Thus, the following assumption is reasonable in practice.

Assumption 1. *The function $b(u_c, p)$ can be considered as a Lipschitz function with respect to the system state p in its practical range.*

3. Online Uncertainty Estimation Based on Extended State Observer

In the system model (6), the model uncertainty always exists due to the parameter uncertainties, such as the temperature variation caused by the thermal effect. To realize satisfying pressure control, the modeling uncertainty should be handled and compensated in the controller design. Thus, an extended state observer is designed in this section to estimate the model uncertainty. Moreover, the bounded stability of the extended state observer is analyzed theoretically.

3.1. Extended State Observer Design

In order to estimate the modeling uncertainty, the term $\phi(t)$ in (6) is extended as an additional state variable, and then the system state is defined as $x = [x_1, x_2]^T$, where $x_1 = p$ and $x_2 = \phi(t)$. Let the derivative of x_2 be denoted as $h(t)$; then, the model (6) can be reformulated as

$$\dot{x}_1 = b(u_c, x_1)u_c + g(x_1) + x_2, \tag{11a}$$
$$\dot{x}_2 = h(t). \tag{11b}$$

Furthermore, the extended model (11a)–(11b) can be rewritten in the following vector form:

$$\dot{x} = Ax + Bu_c + G + H,$$
$$y = Cx, \tag{12}$$

where $A = \begin{bmatrix} 0 & 1 \\ 0 & 0 \end{bmatrix}$, $B = \begin{bmatrix} b(u_c, x_1) \\ 0 \end{bmatrix}$, $G = \begin{bmatrix} g(x_1) \\ 0 \end{bmatrix}$, $H = \begin{bmatrix} 0 \\ h(t) \end{bmatrix}$ and $C = \begin{bmatrix} 1 & 0 \end{bmatrix}$.

Let the estimation of x be denoted as $\hat{x}$. The estimation of B and G is defined as $\hat{B}$ and $\hat{G}$, respectively, where $\hat{B} = \begin{bmatrix} b(u_c, \hat{x}_1) & 0 \end{bmatrix}^T$ and $\hat{G} = \begin{bmatrix} g(\hat{x}_1) & 0 \end{bmatrix}^T$. Then, the model of the extended state observer can be obtained as

$$\dot{\hat{x}} = A\hat{x} + \hat{B}u_c + \hat{G} + L[y - C\hat{x}], \tag{13}$$

where $L = \begin{bmatrix} \beta_1 & \beta_2 \end{bmatrix}^T$ is the observer gain matrix. The values of β_1 and β_2 affect the estimation accuracy of the system state x_1 and the modeling uncertainty x_2, respectively. From Formula (13), we know that the model uncertainty x_2 can be estimated using the measured brake cylinder pressure and the control input. With the estimated x_2, the model (11a) can reflect the pressure dynamics of the brake cylinder more accurately. Moreover, the controller design can take the modeling uncertainty into account explicitly.

3.2. Convergence Analysis of the Extended State Observer

In this section, the convergence analysis of the extended state observer for the brake cylinder pressure control system is provided. Firstly, the estimation error is defined as $\tilde{x} = x - \hat{x}$. In view of Formulas (12) and (13), the dynamics of the estimation error are obtained as

$$\dot{\tilde{x}} = (A - LC)\tilde{x} + \tilde{B}u_c + \tilde{G} + H, \tag{14}$$

where $A - LC = \begin{bmatrix} -\beta_1 & 1 \\ -\beta_2 & 0 \end{bmatrix}$, $\tilde{B} = \begin{bmatrix} b(u_c, x_1) - b(u_c, \hat{x}_1) & 0 \end{bmatrix}^T$, and $\tilde{G} = \begin{bmatrix} g(x_1) - g(\hat{x}_1) & 0 \end{bmatrix}^T$.

Theorem 1. *For the estimation error dynamics (14), if the observer gain matrix L is designed to satisfy the conditions (15) and (29), the estimation error vector $\tilde{x}$ is uniformly bounded, satisfying $\tilde{x} \in D$, $D = \left\{ \tilde{x} \in \Re^2 | \|\tilde{x}\| < r \right\}$ for all $t \geq t_0$, where $r = \max\left\{ \sqrt{\frac{\theta_2}{\theta_1}} \|\tilde{x}(t_0)\|, \frac{\theta_3 h_{\max}}{2E\theta_1} \right\}$, and the parameters $\theta_1, \theta_2, \theta_3, E, h_{\max}$ are defined in the following proof.*

Proof. For the estimation error dynamics (14), if the observer gain matrix L is designed to satisfy the following condition

$$\beta_1 > 0, \beta_2 > \beta_1, \tag{15}$$

all the eigenvalues of matrix $A - LC$ are in the left-half-plane and the matrix $A_e = A - LC$ is Hurwitz. Then, given a positive symmetric matrix Q, there is a positive definite symmetric matrix P that satisfies the following Lyapunov equation:

$$A_e^T P + PA_e = -Q. \tag{16}$$

Define the Lyapunov function of (14) as $V(t, \tilde{x}) = \tilde{x}^T P \tilde{x}$, which satisfies

$$\lambda_{\min}(P)\|\tilde{x}\|^2 \leq V(\tilde{x}) \leq \lambda_{\max}(P)\|\tilde{x}\|^2, \tag{17}$$

$$\left\|\frac{\partial V}{\partial \tilde{x}}\right\| = \left\|2\tilde{x}^T P\right\| \leq 2\|P\|\|\tilde{x}\| \leq 2\lambda_{\max}(P)\|\tilde{x}\|, \tag{18}$$

where $\lambda_{\max}(\cdot)$ denotes the maximum eigenvalues for a matrix and $\lambda_{\min}(\cdot)$ denotes the minimum eigenvalues for a matrix. Define $\theta_1 = \lambda_{\min}(P)$, $\theta_2 = \lambda_{\max}(P)$, and $\theta_3 = 2\lambda_{\max}(P)$. It follows from (14), (16)–(18), that we can obtain the derivative of Lyapunov function V as

$$\begin{aligned}\dot{V} &= \dot{\tilde{x}}^T P \tilde{x} + \tilde{x}^T P \dot{\tilde{x}} \\ &= -\tilde{x}^T Q \tilde{x} + 2\tilde{x}^T P(\tilde{B}u_c + \tilde{G}) + 2\tilde{x}^T PH \\ &\leq -\lambda_{\min}(Q)\|\tilde{x}\|^2 + \theta_3\|\tilde{x}\| \cdot (\tilde{B}u_c + \tilde{G}) + \theta_3\|\tilde{x}\| \cdot H.\end{aligned} \tag{19}$$

From Assumption 1, and according to the definition of $b(u_c, x_1)$, we know that there is a positive constant satisfying the following growth condition:

$$\left\|\tilde{B}\right\| \leq \kappa_1\|\tilde{x}\|. \tag{20}$$

By considering the definition (8) of the practical input u_c, the term $\tilde{B}u_c$ satisfies

$$\left\|\tilde{B}u_c\right\| \leq \kappa_1\|\tilde{x}\|u_m, \tag{21}$$

where u_m denotes the maximum constraint of the control input u.

Moreover, the term $\tilde{G}$ meets

$$\tilde{G} \leq k_t\|\tilde{x}\|. \tag{22}$$

Furthermore, due to the physical constraints, the uncertain matrix H is bounded by

$$\sup_{t_0 \leq \tau \leq t} \|H(\tau)\| \leq h_{\max}, \tag{23}$$

where $h_{\max}$ is a positive constant. Then, Formula (19) can be derived as

$$\dot{V} \leq -\lambda_{\min}(Q)\|\tilde{x}\|^2 + \theta_3(\kappa_1 u_m + k_t)\|\tilde{x}\|^2 + \theta_3\|\tilde{x}\| \cdot h_{\max}. \tag{24}$$

Define $\theta_4 = \lambda_{\min}(Q)$, and $\delta = \kappa_1 u_m + k_t$. Combining Formulas (17) and (24), an upper bound of $\dot{V}$ can be obtained as

$$\dot{V} \leq -\left(\frac{\theta_4}{\theta_2} - \frac{\theta_3}{\theta_1}\delta\right) \cdot V + \theta_3 h_{\max}\sqrt{\frac{V}{\theta_1}}. \tag{25}$$

Define $\Gamma = \sqrt{V}$; then, we can obtain

$$\dot{\Gamma} \leq -\frac{1}{2}\left(\frac{\theta_4}{\theta_2} - \frac{\theta_3}{\theta_1}\delta\right)\Gamma + \frac{\theta_3 h_{\max}}{2\sqrt{\theta_1}}. \tag{26}$$

Solving Formula (26), $\Gamma(t)$ satisfies

$$\Gamma(t) \leq \varphi(t, t_0)\Gamma(t_0) + \frac{\theta_3}{2\sqrt{\theta_1}} \int_{t_0}^{t} \varphi(t, \tau) \cdot h_{\max} d\tau, \tag{27}$$

where $\varphi(t, t_0) = e^{-E(t-t_0)}$, and $E = \frac{\theta_4}{2\theta_2} - \frac{\theta_3}{2\theta_1}\delta$.

Utilizing Formulas (17) and (27), we have

$$\|\tilde{x}(t)\| \leq \sqrt{\frac{\theta_2}{\theta_1}} \|\tilde{x}(t_0)\| e^{-E(t-t_0)} + \frac{\theta_3}{2\theta_1} \int_{t_0}^{t} e^{-E(t-t_0)} \cdot h_{\max} d\tau \tag{28}$$

For the inequality (28), if the following condition

$$E = \frac{\theta_4}{2\theta_2} - \frac{\theta_3}{2\theta_1}\delta > 0, \tag{29}$$

i.e., $\frac{\theta_4}{\theta_2} > \frac{\theta_3}{\theta_1}\delta$ is satisfied with the proper selection of the observer gain matrix L, the inequality (28) can be further derived as

$$\|\tilde{x}(t)\| \leq \sqrt{\frac{\theta_2}{\theta_1}} \|\tilde{x}(t_0)\| e^{-E(t-t_0)} + \frac{\theta_3 h_{\max}}{2E\theta_1} \left[1 - e^{-E(t-t_0)}\right]$$
$$\leq \max\left\{\sqrt{\frac{\theta_2}{\theta_1}} \|\tilde{x}(t_0)\|, \frac{\theta_3 h_{\max}}{2E\theta_1}\right\}. \tag{30}$$

Therefore, it can be concluded that the estimation error $\tilde{x}$ is uniformly bounded, $\tilde{x} \in D$, $D = \{\tilde{x} \in \Re^2 | \|\tilde{x}\| < r\}$ for all $t \geq t_0$. And, its upper bound r relies on the positive parameters θ_1, θ_2, $\|\tilde{x}(t_0)\|$, θ_3, E, and $h_{\max}$, where θ_1, θ_2, θ_3, and E are instrumental variables associated with the eigenvalues of the matrix P. The eigenvalues of the matrix P can be designated by selecting the observer gain matrix L. $\quad\square$

4. Prescribed Performance Pressure Controller Design

In this section, with the estimated model uncertainty, a prescribed performance pressure controller with input saturation compensation is proposed to improve the rapidity and precision of pressure tracking. The pressure tracking error dynamics are first established. Then, a feedback controller is designed to regulate the brake cylinder pressure to the desired values, which includes the simultaneous compensation of the model uncertainty and input saturation by introducing the adaptive parameter technique. A prescribed performance function is introduced into the controller design to guarantee that the desired pressure control accuracy is achieved, which can make the pressure tracking error meet the predetermined bounds. Rigorous stability analysis of the closed-loop control system is also discussed.

4.1. Dynamics of Pressure Tracking Error

Let x_1 and $x_{1d} = p_d$ define the brake cylinder and reference pressures, respectively. The pressure tracking error can be expressed as $e_p = x_1 - x_{1d}$. Then, using Formula (11a), the error dynamics can be described as

$$\dot{e}_p = \dot{x}_1 - \dot{x}_{1d},$$
$$= b(u_c, x_1)u_c + g(x_1) + x_2 - \dot{x}_{1d}. \tag{31}$$

In the train electropneumatic brake system, the reference pressure x_{1d} is given correspondingly according to the specific braking command. Thus, following the characteristic of the practical control system, the reference pressure x_{1d} and its time derivative $\dot{x}_{1d}$ can be assumed to be known and uniformly bounded.

4.2. Prescribed Performance Function

In order to ensure the operation safety of trains, the train brake system needs to provide enough braking force in a short time to ensure that the train braking distance strictly meets the safety constraints. Therefore, to obtain the desired braking behaviors, high requirements are put forward for the transient and steady-state performance of the brake cylinder pressure control. To this end, a prescribed performance function is introduced in this paper. By the prescribed performance function, we can specify that the tracking error converges to a desired small residual set, with the convergence rate no less than a prespecified value, and the maximum overshoot less than a small preset constant. A specific positive decreasing smooth function $\eta(t)$: $\lim_{t\to\infty} \eta(t) = \eta_\infty > 0$ is proposed to describe the prescribed performance. Based on the studies in [22,23], the function $\eta(t)$ in this paper is chosen as

$$\eta(t) = [\eta_0 - \eta_\infty]e^{-k_1 t} + \eta_\infty, \tag{32}$$

where $\eta_0 > \eta_\infty > 0$ and $k_1 > 0$ are the design parameters. Then, the performance of the pressure tracking error e_p can be guaranteed by the following inequality:

$$-\underline{\delta}\eta(t) < e_p < \bar{\delta}\eta(t), \forall t \geq 0, \tag{33}$$

where $\underline{\delta}, \bar{\delta} > 0$ are the design parameters and $-\underline{\delta}\eta(t)$ and $\bar{\delta}\eta(t)$ are denoted as prescribed performance bounds.

According to the above description, we know that the transient and steady-state control performance for the pressure tracking error e_p is ensured by the constraint (33). More specifically, $\bar{\delta}\eta(0)$ determines the upper bound of the maximum overshoot of e_p and $\underline{\delta}\eta(0)$ describes the lower bound of the maximum undershoot of e_p, respectively. In addition, the parameter k_1 in (32) depicts a lower bound on the convergence speed, and η_∞ represents the maximum allowable steady-state error. Thus, desired pressure control objectives can be characterized by setting the parameters $-\underline{\delta}, \bar{\delta}, k_1, \eta_0, \eta_\infty$ in a prior way. The parameter design of the prescribed performance function needs to satisfy two conditions. Firstly, with the parameters, the pressure control should meet the engineering requirements, such as the slight overshoot, setting time, and the steady pressure within a range of ± 3 kPa of the reference value. Secondly, the parameters should be appropriately set to make the system stable according to the principle of parameter setting in [24].

4.3. Controller Design

To achieve the above prescribed performance control as Formula (33), the constrained tracking error behavior should be transformed into an equivalent unconstrained one [16]. For this purpose, an error transformation function is defined as follows:

$$e_p(t) = \eta(t)\Xi(\varepsilon_p), \tag{34}$$

where ε_p is the transformed tracking error and $\Xi(\varepsilon_p)$ is a smooth, strictly increasing function that is defined as

$$\Xi(\varepsilon_p) = \frac{\bar{\delta}e_p^{\varepsilon_p} - \underline{\delta}e_p^{-\varepsilon_p}}{e_p^{\varepsilon_p} + e_p^{-\varepsilon_p}},$$

and $-\underline{\delta} < \Xi(\varepsilon_p) < \bar{\delta}$, $\lim_{\varepsilon_p\to+\infty} \Xi(\varepsilon_p) = \bar{\delta}$, $\lim_{\varepsilon_p\to-\infty} \Xi(\varepsilon_p) = \underline{\delta}$.

Since $\Xi(\varepsilon_p)$ is strictly monotonically increasing, the transformed error ε_p can be expressed as

$$\varepsilon_p = \Xi^{-1}\left(\frac{e_p(t)}{\eta(t)}\right) = \frac{1}{2}\ln\left[\frac{\xi(t) + \underline{\delta}}{\bar{\delta} - \xi(t)}\right], \tag{35}$$

where $\xi(t) = \dfrac{e_p(t)}{\eta(t)}$.

Then, together with Formulas (9) and (31), the time derivative of ε_p can be obtained as

$$
\begin{aligned}
\dot{\varepsilon}_p &= \frac{\partial \Xi^{-1}}{\partial \xi} \dot{\xi} = \frac{1}{2} \left[\frac{1}{\xi + \underline{\delta}} - \frac{1}{\xi - \bar{\delta}} \right] \left(\frac{\dot{e}_p}{\eta} - \frac{e_p \dot{\eta}}{\eta^2} \right) \\
&= \ell \left(b(u_c, x_1) u_c + g(x_1) + x_2 - \dot{x}_{1d} - \frac{e_p \dot{\eta}}{\eta} \right) \\
&= \ell \left(b(u_c, x_1) u + b(u_c, x_1) \Delta u + g(x_1) + x_2 - \dot{x}_{1d} - \frac{e_p \dot{\eta}}{\eta} \right)
\end{aligned}
\tag{36}
$$

where $\ell = \frac{1}{2\eta} \left[\frac{1}{\xi + \underline{\delta}} - \frac{1}{\xi - \bar{\delta}} \right]$ satisfies $0 < \ell < \ell_m$, and ℓ_m is a constant that is calculated based on e_p.

Based on Theorem 1, the modeling uncertainty estimation error $\tilde{x}_2$ satisfies $\|\tilde{x}_2\| \le r$. For Formula (36), considering the input saturation compensation, a feedback control form can be designed as (37) based on the modeling uncertainty estimation $\hat{x}_2$.

$$
\begin{aligned}
u = \frac{1}{\Phi_1} \Bigg[& \frac{-k_o \varepsilon_p}{\ell} - g(x_1) - \hat{x}_2 + \dot{x}_{1d} + \frac{e_p \dot{\eta}}{\eta} \\
& + u_{sc} - \hat{r} \tanh\left(\frac{\varepsilon_p}{\varphi_1} \right) \Bigg],
\end{aligned}
\tag{37}
$$

where k_o is a positive control parameter and Φ_1 is defined by $\Phi_1 = b(u_c, x_1)$. Moreover, the additional term u_{sc} in (37) is developed to efficiently compensate the input saturation $sat(u)$. Similar to reference [21], the additional term u_{sc} can be designed as

$$
u_{sc} = \begin{cases}
\dfrac{-\|\Phi_1\| \varepsilon_p \Pi(x_1) \hat{\zeta}}{\|\varepsilon_p\|}, & \|\varepsilon_p\| \ge \bar{\sigma}, \\[4mm]
0, & \|\varepsilon_p\| < \bar{\sigma},
\end{cases}
\tag{38}
$$

where $\bar{\sigma}$ denotes a designed small positive parameter and $\hat{\zeta}$ represents the estimation value of the uncertain parameter ζ. The corresponding adaptive law $\dot{\hat{\zeta}}$ can be designed as

$$
\dot{\hat{\zeta}} = \ell \left[\Pi(x_1) \|\Phi_1\| \|\varepsilon_p\| - k_q \hat{\zeta} \right],
\tag{39}
$$

where k_q is a designed positive parameter.

Furthermore, for the designed controller (37), $\hat{r}$ represents the estimate of the parameter r, and $\tanh\left(\frac{\varepsilon_p}{\varphi_1} \right)$ is a continuous hyperbolic tangent function for $\varphi_1 > 0$. The term $\hat{r} \tanh\left(\frac{\varepsilon_p}{\varphi_1} \right)$ is introduced to further compensate the system uncertainty. The corresponding adaptive law of $\hat{r}$ can be developed as

$$
\dot{\hat{r}} = \ell \left[\varepsilon_p \tanh\left(\frac{\varepsilon_p}{\varphi_1} \right) - k_r \hat{r} \right],
\tag{40}
$$

where k_r is a designed positive parameter.

4.4. Stability Analysis

This section discusses the stability of the closed-loop brake cylinder pressure control system. For the brake cylinder pressure control system, given the initial pressure $p(0)$, we can choose proper $\bar{\delta}$, $\underline{\delta}$, and $\eta(0)$ to make the initial tracking error satisfy $-\underline{\delta} \eta(0) < e_p(0) < \bar{\delta} \eta(0)$. The control performance of the tracking error can be improved by tuning the parameters $\bar{\delta}$, $\underline{\delta}$, and $\eta(t)$. For the transformed system and the designed pressure controller, one can conclude that the transformed error ε_p must be bounded to achieve a good pressure tracking performance. Thus, the desired pressure tracking control can be achieved if the transformed

system is stable. Before proceeding with the stability analysis, Lemmas 1 and 2 are given first. Then, the main result of the proposed pressure control scheme with the prescribed performance function is established in Theorem 2.

Lemma 1 ([16]). *The tracking error dynamics (31) are invariant through the error transformation of (35). Thus, it is valid that the control issue of (31) with the constrained condition (33) is transformed into stabilizing the transformed error ε_p. If ε_p is bounded, then the prescribed performance of e_p as shown in (33) is satisfied.*

Lemma 2 ([25]). *For a continuous function $V_1(t) \geq 0$, it satisfies $V_1(t_0)$ being bounded. If $\dot{V}_1 \leq -\bar{p}_1 V_1 + \bar{p}_2$, $V_1(t)$ is bounded with $\bar{p}_1 > 0$ and $\bar{p}_2$ being a constant parameter.*

Theorem 2. *Consider the system (6) with uncertainty and nonlinearity; by designing the prescribed performance-function-based control law (37), the transformed error ε_p converges to a small set around zero, and the tracking error e_p satisfies the prescribed performance constraint (33).*

Proof. It follows from (36) and (37) that

$$\dot{\varepsilon}_p = -k_o \varepsilon_p + \ell \tilde{x}_2 - \ell \hat{r} \tanh\left(\frac{\varepsilon_p}{\varphi_1}\right) + \ell u_{sc} + \ell \Phi_1 \Delta u, \tag{41}$$

where $\tilde{x}_2 = x_2 - \hat{x}_2$.

Define $\tilde{\zeta} = \zeta - \hat{\zeta}$ and $\tilde{r} = r - \hat{r}$, and the Lyapunov function is given by

$$V_1 = \frac{1}{2}\varepsilon_p^2 + \frac{1}{2}\tilde{r}^2 + \frac{1}{2}\tilde{\zeta}^2. \tag{42}$$

Considering $\dot{\tilde{\zeta}} = -\dot{\hat{\zeta}}$, $\dot{\tilde{r}} = -\dot{\hat{r}}$ and Formulas (38) and (41), the derivative of the Lyapunov function can be obtained as

$$\begin{aligned} \dot{V}_1 &= \dot{\varepsilon}_p \varepsilon_p + \dot{\tilde{r}}\tilde{r} + \dot{\tilde{\zeta}}\tilde{\zeta} \\ &= -k_o \varepsilon_p^2 + \ell \tilde{x}_2 \varepsilon_p - \ell \hat{r}\varepsilon_p \tanh\left(\frac{\varepsilon_p}{\varphi_1}\right) \\ &\quad -\ell \frac{\|\Phi_1\|\varepsilon_p^2 \Pi(x_1)\hat{\zeta}}{\|\varepsilon_p\|} + \ell \Phi_1 \Delta u \varepsilon_p - \dot{\hat{r}}\tilde{r} - \dot{\hat{\zeta}}\tilde{\zeta}. \end{aligned} \tag{43}$$

According to Theorem 1, the term $|\tilde{x}_2| < r$. With the adaptive laws in Formulas (39) and (40), one can obtain

$$\dot{V}_1 \leq -k_o \varepsilon_p^2 + \ell r |\varepsilon_p| - \ell r \varepsilon_p \tanh\left(\frac{\varepsilon_p}{\varphi_1}\right) + \ell k_r \hat{r}\tilde{r} + \ell k_q \hat{\zeta}\tilde{\zeta}. \tag{44}$$

Introducing the property $0 \leq |z_1| - z_1 \tanh\left(\frac{z_1}{\bar{\gamma}}\right) \leq k_m \bar{\gamma}$, $k_m = 0.2785$ for $\forall \bar{\gamma} > 0$ [25], the following inequality (45) can be obtained.

$$\ell r \left[|\varepsilon_p| - \varepsilon_p \tanh\left(\frac{\varepsilon_p}{\varphi_1}\right)\right] \leq \ell r k_m \varphi_1. \tag{45}$$

Further, using Young's inequality, one can obtain that

$$\begin{aligned} \ell k_r \hat{r}\tilde{r} &\leq \frac{\ell k_r}{2}r^2 - \frac{\ell k_r}{2}\tilde{r}^2, \\ \ell k_q \hat{\zeta}\tilde{\zeta} &\leq \frac{\ell k_q}{2}\zeta^2 - \frac{\ell k_q}{2}\tilde{\zeta}^2. \end{aligned} \tag{46}$$

Substituting (45) and (46) into (44) yields

$$\dot{V}_1 \leq -k_o\varepsilon_p^2 - \frac{\ell k_r}{2}\tilde{r}^2 - \frac{\ell k_q}{2}\tilde{\zeta}^2 + \ell_m r k_m \varphi_1 + \frac{\ell_m k_r}{2}r^2 + \frac{\ell_m k_q}{2}\zeta^2$$
$$\leq -\bar{K}_1 V_1 + \bar{D}_1, \tag{47}$$

where $\bar{K}_1$ is defined as $\bar{K}_1 = \min\{2k_o, \ell k_r, \ell k_q\}$, and $\bar{D}_1$ is defined as $\bar{D}_1 = \ell_m r k_m \varphi_1 + \frac{\ell_m k_r}{2}r^2 + \frac{\ell_m k_q}{2}\zeta^2$.

Therefore, based on Lemma 2, one can obtain that V_1 is ultimately bounded. By utilizing the comparison principle, the following inequality holds:

$$V_1(t) \leq \left[V_1(t_0) - \frac{\bar{D}_1}{\bar{K}_1}\right]e^{-\bar{K}_1 t} + \frac{\bar{D}_1}{\bar{K}_1}. \tag{48}$$

Thus, we can obtain that V_1 is uniformly ultimately bounded. The transformation error ε_p is bounded and its upper bound depends on the control parameters and the estimation performance of the designed extended state observer. In addition, due to the inherent properties of the function $\Xi(\varepsilon_p)$ and the error transformation function (34), we can obtain that the tracking error e_p satisfies the prescribed performance bounds; that is, $-\underline{\delta}\eta(t) < e_p < \bar{\delta}\eta(t)$. This completes the proof. □

5. Experimental Validation

In this section, experiments are made on the test platform of the brake cylinder pressure control system to validate the effectiveness of the proposed method. The experimental platform and setup are described first. Then, the experimental results are presented and analyzed.

5.1. Experimental Setup

Figure 2 shows the brake cylinder pressure control platform. In the experimental platform, the proposed prescribed performance pressure controller is operated in the brake control unit. Two high-speed on/off solenoid valves (MAC 35A-ACA-DDFA-1BA) are controlled to be open or closed so that the brake cylinder pressure can track the reference values. The pressure sensors (Keller PA-21Y) are used to measure the pressure of the brake cylinder and the main air reservoir. In addition, the air drier is a system accessory that can filter out water from the air. Moreover, Figure 3 shows the block diagram of the experimental platform, which describes the relationship among the components in the experimental platform.
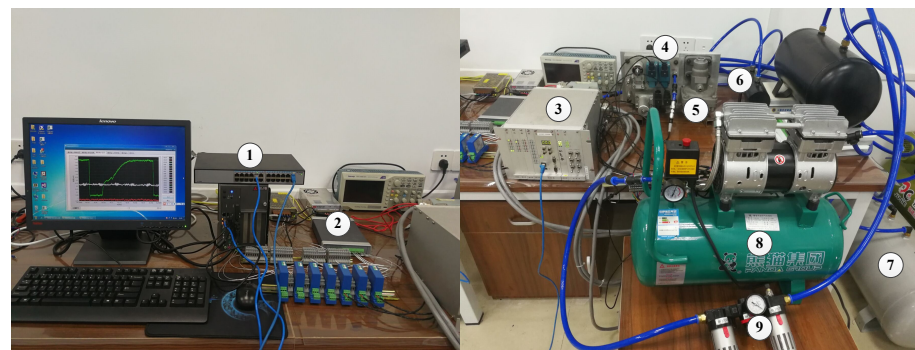
Figure 2. The experimental platform for testing the brake cylinder pressure control method. (1) Industrial personal computer; (2) data acquisition card; (3) brake control unit; (4) supply valve and exhaust valve; (5) pressure sensor; (6) brake cylinder; (7) main air reservoir; (8) air compressor; (9) air dryer.
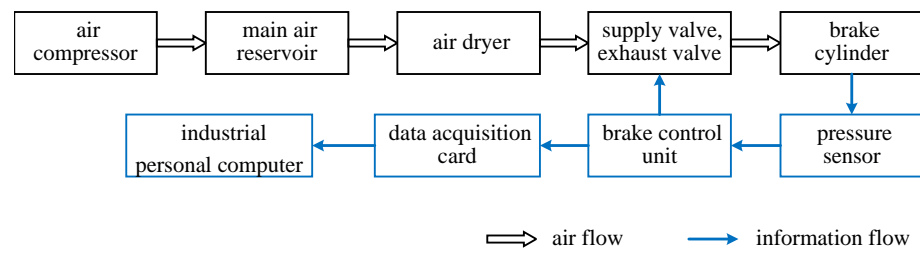
Figure 3. The block diagram of the experimental platform.

The model parameters of the electropneumatic brake system are provided in Table 1.

Table 1. Model parameters of the electropneumatic brake system.

Parameters	Values	Parameters	Values
V	1.2 L	R	287 J·(Kg·K)$^{-1}$
A_1	6.2 mm^2	A_2	5.7 mm^2
T	293.15 K	γ	1.4
p_s	700 kPa	p_a	101.325 kPa
C_d	0.64	k_t	0.001 (1/s)

The other controller parameters are set as $\beta_1 = 1860$, $\beta_2 = 10100$, $k_q = 3.5$, $k_r = 3.2$, $k_o = 1.8$. The control parameters of the prescribed performance function are given by $\eta_0 = 200$, $\eta_\infty = 0.3$, $\underline{\delta} = 1.01$, $\bar{\delta} = 1.04$, $k_1 = 1.25$ in the braking mode, and $\eta_0 = 300$, $\eta_\infty = 0.3$, $\underline{\delta} = 1.03$, $\bar{\delta} = 1.01$, $k_1 = 1.2$ in the releasing mode.

5.2. Experimental Results and Analysis

With the electropneumatic brake system shown in Figure 1, the train has two commonly used operation modes including the braking mode and the releasing mode, and the experiments are conducted under the two modes. Moreover, the following three controllers are compared.

PI: The proportional–integral controller, which is widely used in the practical electropneumatic brake system due to its easy deployment, and thus is treated as a benchmark controller for comparison. For a fair comparison, the PI gains are set as $k_P = 1.6/\left(3 \times 10^5\right)$, $k_I = 0.001/\left(3 \times 10^5\right)$.

PPC: The prescribed performance pressure tracking controller without the extended state observer, and PPC for short here.

Observer-based PPC: The prescribed performance pressure tracking controller with the extended state observer proposed in this paper, and OPPC for short here.

The following performance indices are used to evaluate the quality of each controller.
(1)　RMSE: The root mean squared error (RMSE) is defined as

$$\text{RMSE} = \sqrt{\frac{1}{N} \sum_{i=1}^{N} \left(e_p(i)\right)^2}, \tag{49}$$

where N is the sample number.
(2)　SSE: The steady-state error (SSE), which is used as an index of measure of tracking accuracy.
(3)　ST: The settling time (ST), which is used to evaluate the rapidity of the pressure tracking. It is defined as the time required for the pressure curve to reach and stay within a range of ± 3 kPa of the reference value in this paper.

(4)   SN: The switching number, which is used as a numerical measure of the switching activity of the on/off solenoid valve. It is defined as the total number of switches of the two solenoid valves.

Detailed experimental results and performance comparisons of three controllers are provided as follows.

5.2.1. Braking Experiment

In the braking mode, the brake cylinder pressure should be increased to a given reference pressure by controlling two solenoid valves. In this experiment, the brake cylinder pressure is set to increase from 0 kPa to 300 kPa. Figure 4 presents the comparative pressure tracking results of three control methods. As shown in Figure 4, three controllers can make the pressure of the brake cylinder increase quickly and reach the reference pressure within only 1 s. However, the PI controller makes the pressure have large fluctuations during 1~8.2 s. Although the pressure curve under the PPC method is smoother than that under the PI controller, it has a larger steady-state error compared with that under the proposed controller. The proposed control method, i.e., OPPC, shows the best pressure control performance. This is because the proposed controller addresses the system uncertainty in real time and switches the valves appropriately to achieve fast and precise pressure tracking.
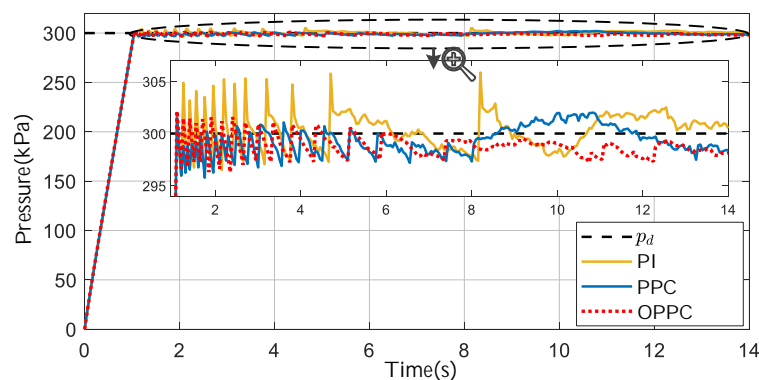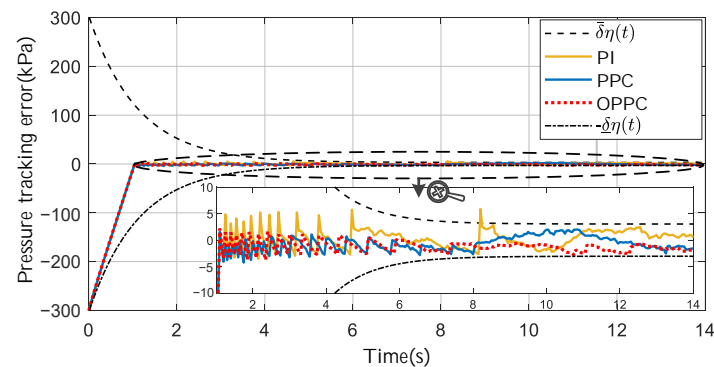

Figure 4. The comparative pressure tracking results of the PI, the PPC, and the OPPC methods under the braking mode.

The pressure tracking errors of the three control methods are shown in Figure 5. From this figure, it can be found that the error curve fluctuates violently for the PI method, which leads to a larger overshoot and steady-state error. Compared with the PI method, the pressure tracking errors of the PPC and the OPPC methods are always within the prescribed performance bounds, which makes the pressure have smaller overshoot and steady-state errors. Moreover, the proposed control method makes the pressure converge to the range of ± 3 kPa of the reference pressure more quickly than the PPC method. The compared tracking errors in Figure 5 further verify the superiority of the proposed method.
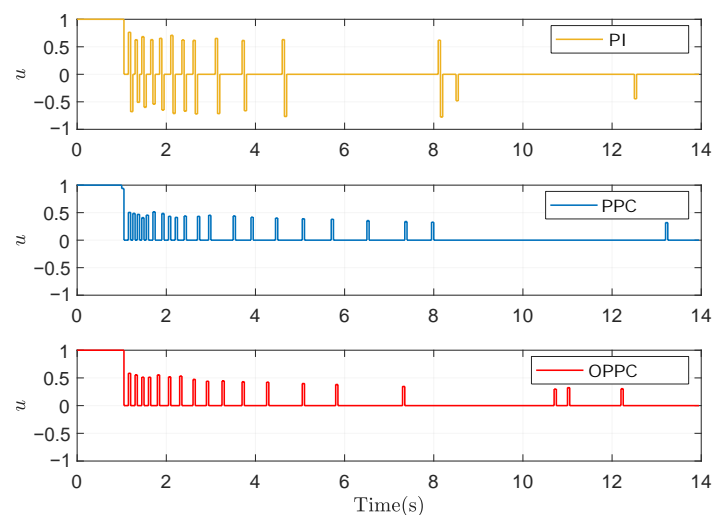
Figure 6 shows the comparative PWM signals of three control methods under the braking mode. $[-1, 0)$ means that only the exhaust valve is open, $(0, 1]$ means that only the supply valve is open, and 0 means that two valves are closed. From the results, three controllers can generate the same control signal to open the supply valve during 0~1 s, and then the pressure rises similarly during this period. However, after the pressure reaches the reference pressure at 1 s, the proposed pressure controller can calculate the control signals correctly because of its adaptivity to the system uncertainty, and the PWM duty cycles are smaller than the ones of the PI controller. The small PWM duty cycle leads to a slight adjustment in the pressure, which can reduce the effect of the temperature variation and other uncertainties on the pressure and make the pressure converge to the reference value quickly. Furthermore, since the uncertainty is compensated in the control input, the values of the duty cycles are larger under the OPPC method compared with the PPC method, but they lead to faster convergence of the pressure and fewer switching times of solenoid

valves. In addition, the low number of switching times can result in the short energizing time of solenoid valves, slowing down the aging of the solenoid valves.


Figure 5. The comparative pressure tracking errors of the PI, the PPC, and the OPPC methods under the braking mode.


Figure 6. The comparative PWM signals among the PI, the PPC, and the OPPC methods under the braking mode.

Figures 7 and 8 show the estimated results of x_1 and x_2, respectively. Figure 7 shows the comparison between the real x_1 and its estimation $\hat{x}_1$, from which it can be found that the obtained $\hat{x}_1$ is accurate enough. From Figure 8, it can be found that, during the whole pressure control process, the system uncertainty such as the temperature variation shows significant changes, causing the pressure to fluctuate notably. Thus, it is necessary to estimate the uncertainty online to compensate for the control input and improve the controller performance.
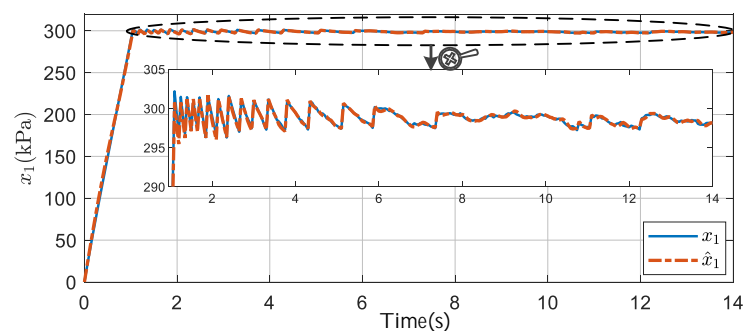
Figure 7. The comparison between x_1 and $\hat{x}_1$ under the braking mode.
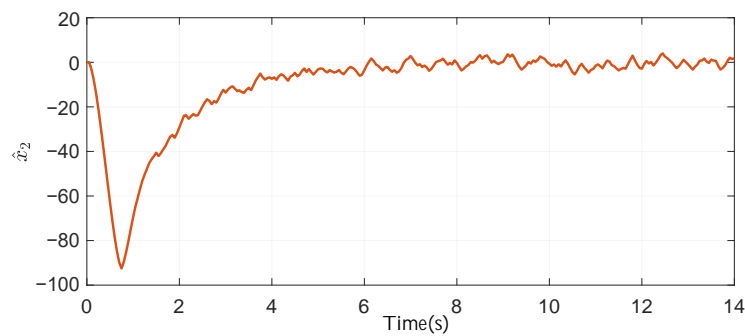
**Figure 8.** The estimation of system uncertainties x_2 under the braking mode.

Table 2 also summarizes the control performance comparisons of three methods in the braking experiment based on the quantified indicators of RMSE, SSE, ST, and SN. The results also present that the proposed controller OPPC can provide the best pressure control performance. The performance comparisons also verify the effectiveness and superiority of the proposed control method.

Table 2. Performance comparisons of PI, PPC, and OPPC controllers under the braking mode.

Controller	RMSE	SSE	ST	SN
PI	48.2443	2.88	4.75	26
PPC	48.1951	2.82	3.6	22
OPPC	48.0397	2.59	2.65	18

5.2.2. Releasing Experiment

When the train is in the releasing mode, the pressure controller should control two solenoid valves to make the brake cylinder discharge and reach the reference pressure. In this experiment, the initial pressure of the brake cylinder is set to 400 kPa and the reference pressure is set to 100 kPa. Figure 9 presents the comparative pressure tracking results of the brake cylinder controlled by three controllers. From Figure 9, the pressure reaches the reference value until 7 s and exhibits distinct undershoot and overshoot at 10.5 s under the PI controller. Compared with the PI controller, the pressure controlled by the other two controllers responds more quickly during 4∼7 s but results in a longer settling time due to distinct chattering, and displays smoother tracking during 7∼14 s. Among the three controllers, the proposed controller OPPC provides the most rapid and accurate pressure tracking results.
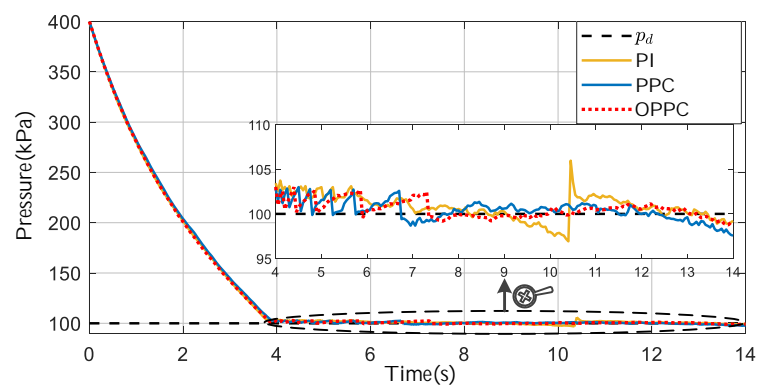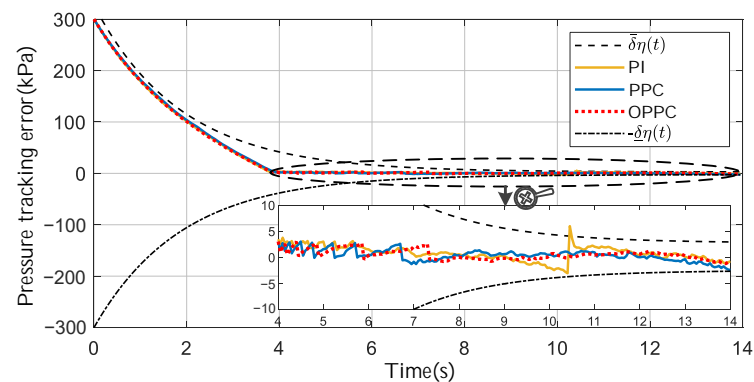

Figure 9. The comparative pressure tracking results among the PI, the PPC, and the OPPC method under the releasing mode.

The pressure tracking errors of three controllers are plotted in Figure 10. From this figure, it can be found that the tracking error under the PI control method is beyond the

prescribed performance bounds at 10.5 s. Although the tracking error under the PPC method satisfies the prescribed performance bounds, the error curve has more fluctuations and there is a larger steady-state error compared with that of the proposed control method. With the proposed OPPC method, the pressure error curve is smooth and the steady-state error is small. The compared pressure tracking errors further show that the proposed method can achieve better control performance.

Figure 11 shows the comparison of the PWM signals among three controllers, where $[-1,0)$ means that the exhaust valve is open and 0 means that the exhaust valve and the supply valve are both closed. For the three controllers, the exhaust valve becomes open during 0∼3.85 s after the braking command is given and then the pressure of the brake cylinder decreases. A change in the duty ratio means a switch in the solenoid valve in Figure 11. With the PI controller, the values of duty cycles are small but result in many switches in solenoid valves. Compared with the PI controller, the switching times of the solenoid valves of the other two controllers are fewer. For the proposed OPPC method, since the estimated model uncertainty compensates for its control input, it can calculate the control signals more appropriately. Then, the least amount of switching times of solenoid valves is obtained when compared with the other two controllers. The proposed pressure controller helps lengthen the lifetime of the valves.


Figure 10. The comparative pressure tracking errors among the PI, the PPC, and the OPPC method under the releasing mode.
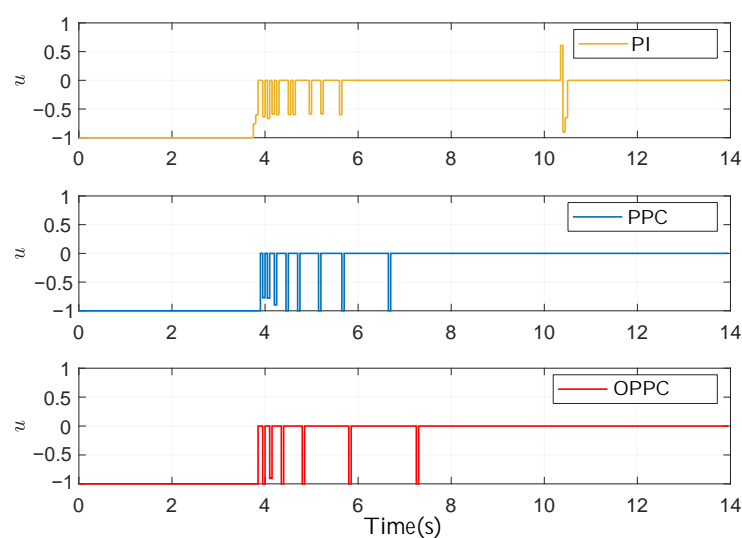

Figure 11. The comparative PWM signals among the PI, the PPC, and the OPPC method under the releasing mode.

Figures 12 and 13 show the estimated x_1 and x_2, respectively. In Figure 12, we can see that the estimated x_1 can match the real x_1 well. From Figure 13, it can be found that the

uncertainty in the brake cylinder pressure system also shows significant changes during the air discharging. Thus, it is necessary to estimate the uncertainty online to improve the performance of the pressure controller.
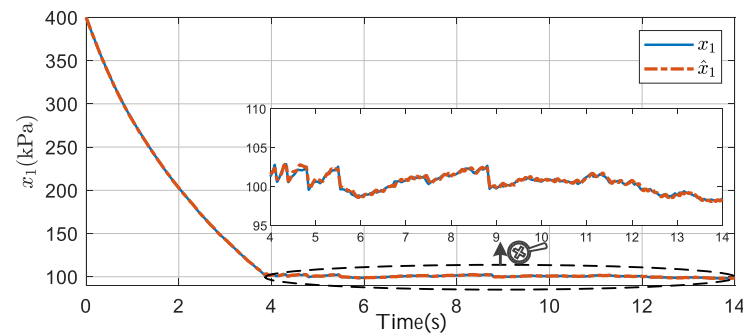
Figure 12. The comparison between x_1 and $\hat{x}_1$ under the releasing mode.
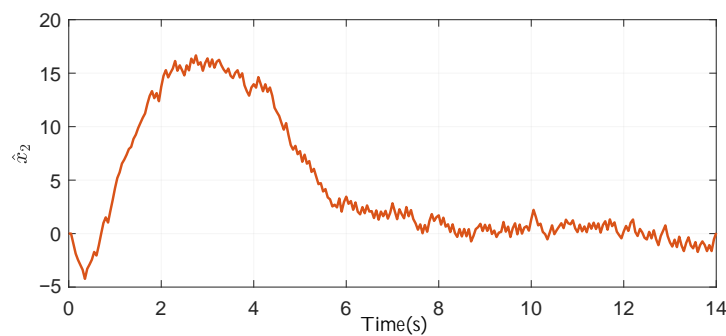
Figure 13. The estimation of system uncertainties x_2 under the releasing mode.

Table 3 summarizes the control performance comparisons of three methods in the releasing experiment based on the quantified indicators of RMSE, SSE, ST, and SN. The results demonstrate that the proposed controller OPPC provides the best pressure control performance, which is reflected by its minimal values in four performance metrics. The quantified performance comparisons further verify the effectiveness of the proposed control method.

Table 3. Performance comparisons of PI controller, PPC controller, and OPPC controller under the releasing mode.

Controller	RMSE	SSE	ST	SN
PI	78.4979	3.0	3.85	14
PPC	78.4401	2.58	3.9	8
OPPC	77.2698	2.37	3.75	6

6. Conclusions

This paper proposes a prescribed performance pressure control method with online model uncertainty estimation for a train electropneumatic brake system. The proposed method overcomes the challenge caused by the nonlinearity, uncertainties, and input saturation, guaranteeing the desired control performance. Based on the designed extended state observer, an accurate uncertainty estimation of the brake cylinder is first achieved in real time. The desired pressure tracking performance is then ensured by introducing the prescribed performance function and parameter adaptive method in the controller design. Rigorous convergence analysis of the designed observer and stability analysis of the closed-loop pressure control system are presented. Comparative experimental results verify the effectiveness and superiority of the proposed pressure control method. In this

research, it is worth noting that the estimation of the system uncertainties directly affects the performance of the proposed control strategy. Hence, the determination of the optimal gains of an extended state observer will be another possible topic for further work.

Institutional Review Board Statement: Not applicable.

Informed Consent Statement: Not applicable.

Data Availability Statement: Not applicable.

Conflicts of Interest: The authors declare no conflict of interest.

References

1. Liu, Z.; Wang, C.; Yang, X.; Zhang, N.; Liu, F.; Zhang, B. Time Series Multi-Step Forecasting Based on Memory Network for the Prognostics and Health Management in Freight Train Braking System. *IEEE Trans. Intell. Transp. Syst.* **2023**, *24*, 8149–8162. [CrossRef]
2. Rahman, F.; Akanda, M.S. Effect of Heat Transfer Through Walls on Response of Pneumatic System. *Arab. J. Sci. Eng.* **2019**, *44*, 7753–7765 . [CrossRef]
3. Shan, T.; Li, L.; Wu, X.; Cheng, S. Pressure control based on reinforcement learning strategy of the pneumatic relays for an electric-pneumatic braking system. *Proc. Inst. Mech. Eng. Part J. Automob. Eng.* **2022**, *237* , 1–12. [CrossRef]
4. Mazare, M.; Taghizadeh, M.; Kazemi, M.G. Optimal hybrid scheme of dynamic neural network and PID controller based on harmony search algorithm to control a PWM-driven pneumatic actuator position. *J. Vib. Control* **2018**, *24*, 3538–3554. [CrossRef]
5. Luo, Z.; Wu, M.; Zuo, J. Sliding mode pressure controller for an electropneumatic brake: Part II: Parameter identification and controller tests. *Proc. Inst. Mech. Eng. Part J. Syst. Control Eng.* **2018**, *232*, 583–591. [CrossRef]
6. Azahar, M.I.P.; Irawan, A.; Ismail, R.R. Self-tuning hybrid fuzzy sliding surface control for pneumatic servo system positioning. *Control Eng. Pract.* **2021**, *113*, 104838. [CrossRef]
7. Qi, H.; Bone, G.M.; Zhang, Y. Position Control of Pneumatic Actuators Using Three-Mode Discrete-Valued Model Predictive Control. *Actuators* **2019**, *8*, 56. [CrossRef]
8. Zhang, R.; Peng, J.; Li, H.; Chen, B.; Liu, W.; Huang, Z.; Wang, J. A predictive control method to improve pressure tracking precision and reduce valve switching for pneumatic brake systems. *IET Control Theory Appl.* **2021**, *15*, 1389–1403. [CrossRef]
9. Wang, Y.; Liu, X.J.; Zhao, H. Speeding up soft pneumatic actuators through pressure and flow dynamics modeling and optimization. *Extrem. Mech. Lett.* **2022**, *57*, 101914. [CrossRef]
10. Bigras, P. Sliding-Mode Observer as a Time-Variant Estimator for Control of Pneumatic Systems. *J. Dyn. Syst. Meas. Control* **2005**, *127*, 499–502. [CrossRef]
11. Ayadi, A.; Hajji, S.; Smaoui, M.; Chaari, A.; Farza, M. Dynamic high-gain observer to estimate pneumatic actuator temperatures. *J. Dyn. Syst. Meas. Control* **2016**, *138*, 1–7. [CrossRef]
12. Han, J. From PID to active disturbance rejection control. *IEEE Trans. Ind. Electron.* **2009**, *56*, 900–906. [CrossRef]
13. Dao, Q.T.; Dinh, V.V.; Trinh, M.C.; Tran, V.C.; Nguyen, V.L.; Duong, M.D.; Bui, N.T. Nonlinear Extended Observer-Based ADRC for a Lower-Limb PAM-Based Exoskeleton. *Actuators* **2022**, *11*, 369. [CrossRef]
14. Chen, B.; Huang, Z.; Zhang, R.; Jiang, F.; Liu, W.; Li, H.; Wang, J.; Peng, J. Adaptive slip ratio estimation for active braking control of high-speed trains. *ISA Trans.* **2020**, *112*, 302–314. [CrossRef] [PubMed]
15. Razmjooei, H.; Palli, G.; Abdi, E.; Terzo, M.; Strano, S. Design and experimental validation of an adaptive fast-finite-time observer on uncertain electro-hydraulic systems. *Control Eng. Pract.* **2023**, *131*, 105391. [CrossRef]
16. Bechlioulis, C.P.; Rovithakis, G.A. Robust adaptive control of feedback linearizable MIMO nonlinear systems with prescribed performance. *IEEE Trans. Autom. Control* **2008**, *53*, 2090–2099. [CrossRef]
17. Verginis, C.K.; Bechlioulis, C.P.; Soldatos, A.G.; Tsipianitis, D. Robust trajectory tracking control for uncertain 3-dof helicopters with prescribed performance. *IEEE/ASME Trans. Mechatron.* **2022**, *27*, 3559–3569. [CrossRef]
18. Song, X.; Wu, C.; Stojanovic, V.; Song, S. 1 bit encoding–decoding-based event-triggered fixed-time adaptive control for unmanned surface vehicle with guaranteed tracking performance. *Control Eng. Pract.* **2023**, *135*, 105513. [CrossRef]
19. Nguyen, T.; Leavitt, J.; Jabbari, F.; Bobrow, J. Accurate sliding-mode control of pneumatic systems using low-cost solenoid valves. *IEEE/ASME Trans. Mechatron.* **2007**, *12*, 216–219. [CrossRef]

20. Hodgson, S.; Tavakoli, M.; Pham, M.T.; Leleve, A. Nonlinear discontinuous dynamics averaging and PWM-based sliding control of solenoid-valve pneumatic actuators. *IEEE/ASME Trans. Mechatron.* **2015**, *20*, 876–888. [CrossRef]

21. Chen, M.; Wu, Q.; Jiang, C.; Jiang, B. Guaranteed transient performance based control with input saturation for near space vehicles. *Sci. China Inf. Sci.* **2014**, *57*, 1–12. [CrossRef]

22. Bechlioulis, C.P.; Rovithakis, G.A. Adaptive control with guaranteed transient and steady state tracking error bounds for strict feedback systems. *Automatica* **2009**, *45*, 532–538. [CrossRef]

23. Zhang, C.; Ma, G.; Sun, Y.; Li, C. Observer based active vibration control of flexible space structures with prescribed performance. *J. Frankl. Inst.* **2020**, *357*, 1400–1419. [CrossRef]

24. Na, J.; Chen, Q.; Ren, X.; Guo, Y. Adaptive prescribed performance motion control of servo mechanisms with friction compensation. *IEEE Trans. Ind. Electron.* **2014**, *61*, 486–494. [CrossRef]

25. Guo, G.; Li, D. Adaptive sliding mode control of vehicular platoons with prescribed tracking performance. *IEEE Trans. Veh. Technol.* **2019**, *68*, 7511–7520. [CrossRef]